Lasers Med Sci (2017) 32:1469–1477
DOI 10.1007/s10103-017-2267-x

ORIGINAL ARTICLE

Gold-coated magnetic nanoparticle as a nanotheranostic agent for magnetic resonance imaging and photothermal therapy of cancer

Nazila Eyvazzadeh[1] · Ali Shakeri-Zadeh[2] · Reza Fekrazad[3,4] · Elahe Amini[5] · Habib Ghaznavi[6] · S. Kamran Kamrava[4,7]

Received: 16 September 2016 / Accepted: 16 June 2017 / Published online: 3 July 2017

Abstract Because of their great scientific and technological potentials, iron oxide nanoparticles (IONPs) have been the focus of extensive investigations in biomedicine over the past decade. Additionally, the surface plasmon resonance effect of gold nanoparticles (AuNPs) makes them a good candidate for photothermal therapy applications. The unique properties of both IONPs (magnetic) and AuNPs (surface plasmon resonance) may lead to the development of a multi-modal nanoplatform to be used as a magnetic resonance imaging (MRI) contrast agent and as a nanoheater for photothermal therapy. Herein, core–shell gold-coated IONPs (Au@IONPs) were synthesized and investigated as an MRI contrast agent and as a light-responsive agent for cancer photothermal therapy.

The synthesized Au@IONPs were characterized by UV–visible spectroscopy, transmission electron microscopy (TEM), dynamic light scattering (DLS), and zeta potential analysis. The transverse relaxivity (r_2) of the Au@IONPs was measured using a 3-T clinical MRI scanner. Through a 3-(4,5-dimethylthiazol-2-yl)-2,5-diphenyltetrazolium bromide (MTT) assay, the cytotoxicity of the Au@IONs was examined on a KB cell line, derived from the epidermal carcinoma of a human mouth. Moreover, the photothermal effects of Au@IONPs in the presence of a laser beam (λ = 808 nm; 6.3 W/cm^2; 5 min) were studied.

The results show that the Au@IONPs are spherical with a hydrodynamic size of 33 nm. A transverse relaxivity of 95 mM^{-1} S^{-1} was measured for the synthesized Au@IONPs. It is evident from the MTT results that no significant cytotoxicity in KB cells occurs with Au@IONPs. Additionally, no significant cell damage induced by the laser is observed. Following the photothermal treatment using Au@IONPs, approximately 70% cell death is achieved. It is found that cell lethality depended strongly on incubation period and the Au@IONP concentration.

The data highlight the potential of Au@IONPs as a dual-function MRI contrast agent and photosensitizer for cancer photothermal therapy.

Keywords Magnetic nanoparticles · Gold nanoparticles · Core–shell nanoparticles · MRI contrast agent · Cancer · Photothermal therapy

✉ Habib Ghaznavi
ghaznavih@yahoo.com

✉ S. Kamran Kamrava
skkamrava@yahoo.com

[1] Radiation Research Center, Allied Medical Sciences School, AJA University of Medical Sciences, Tehran, Iran

[2] Medical Physics Department, School of Medicine, Iran University of Medical Sciences (IUMS), Tehran, Iran

[3] Department of Periodontology, Dental Faculty - Laser Research Center in Medical Sciences, AJA University of Medical Sciences, Tehran, Iran

[4] International Network for Photo Medicine and Photo Dynamic Therapy (INPMPDT), Universal Scientific Education and Research Network (USERN), Tehran, Iran

[5] ENT and Head & Neck Research Center and Department, Iran University of Medical Sciences (IUMS), Tehran, Iran

[6] Cellular and Molecular Research Center, Zahedan University of Medical Sciences (ZaUMS), Zahedan, Iran

[7] Applied Biophotonics Research Center, Science and Research Branch, Islamic Azad University, Tehran, Iran

Introduction

Cancer is a disease of the cell in which the normal control mechanisms of cell growth and proliferation are disturbed [1, 2]. Presently, several novel nanotechnology-based methods for cancer diagnosis and therapy are under

investigation, and the synthesis of various nanoparticles with particular properties has been the focus of extensive research over the past decade [3–5]. Among these nanoparticles, iron oxide nanoparticles (IONPs) and gold nanoparticles (AuNPs) are of particular interest for developing unique systems with high potential in cancer diagnosis and therapy [6–8].

IONPs may simultaneously offer various functions. As a multi-functional nanoparticle, IONP can be considered as a good (a) drug carrier, (b) radiosensitizer in radiotherapy, (c) magnetic hyperthermia agent, and (d) contrast agent in magnetic resonance imaging (MRI) even at low concentrations [6, 9–11]. Normal tissues and tumors differ only slightly in relaxation time, and MRI alone may not be accurate enough to enable a proper diagnosis. MRI contrast agents clarify images to improve the interpretation. The development of new contrast agents based on new nanomaterials is a fascinating field of research that focuses on improving MRI techniques for the early detection of disease. IONPs have been extensively employed as a negative contrast agent, altering the MR signal by reducing the T_2^* and T_2 values through de-phasing of the transverse magnetization [12]. The polymeric surface modification of IONPs increases their circulation half-life in blood and decreases their oxidation and toxicity in biological media [13, 14]. Gold shell coatings may also be useful in this regard due to their high chemical stability and biocompatibility. In addition, the plasmon-derived optical resonances of gold shells in the visible and near-infrared region (NIR) allow them to serve as diagnostic and therapeutic agents simultaneously [15, 16].

Gold nanoparticles (AuNPs) have represented a completely novel technology in the field of nanoparticle-based cancer therapy. AuNPs have unique properties involving the absorption of laser light that make them suitable to be used in cancer photothermal treatment. When a laser beam is irradiated to AuNPs, light is absorbed by the nanoparticles and then the free electrons exhibit a collective coherent oscillation around the nanoparticle surface [16, 17]. This coherent oscillation is induced as a result of a well-known phenomenon called localized surface plasmon resonance [18]. The absorbed light is converted into heat through a series of photo-physical processes [19]. In fact, the light is quickly converted to heat, and a hot metallic lattice is formed by (a) electron–electron relaxation occurring on femto-seconds and (b) electron–phonon relaxation occurring on the picoseconds. The hot metallic lattice then cools off by phonon–phonon relaxation [18]. As a result, if cancer cells are loaded by AuNPs and then irradiated with appropriate laser (even with the energy as low as 100 nJ), the lattice temperature is highly increased [18]. The generated heat is dissipated from the nanoparticles into the surrounding environment, and the released heat from nanoparticles may cause fatal damage to cancer cells through local overheating effects [20]. Accordingly, AuNPs are considered to be an elegant photothermal agent in therapeutic applications, especially in cancer treatment [21].

Considering the mentioned properties of IONPs and AuNPs, it seems that combination of both nanoparticles in a single nanocomplex may offer good potentials in the fields of cancer diagnosis and therapy. Recently, core–shell gold-coated IONP (Au@IONP) nanocomplex has been introduced as a new class of multi-functional nanoparticles in the various areas of cancer nanotechnology such as cancer cell imaging, radiation therapy, and photothermal therapy [22]. In this study, after the preparation of core–shell Au@IONPs, the capability of this nanocomplex in enhancing the contrast of MR images and its photothermal effects on KB cell line were assessed. Moreover, the effects of incubation time and nanoparticle concentration on cell lethality and the contrast of MR images were determined.

Materials and methods

Materials

Iron (II) chloride tetrahydrate (>99%), iron (III) chloride hexahydrate (>99%), ammonia (32%), methanol (99.9%), and toluene (>99%) were purchased from Merck (Darmstadt, Germany). (3-Aminopropyl)trimethoxysilane (97%) was purchased from Fluka (Switzerland). Gold(III) chloride solution was purchased from Sigma (USA). Deionized water was used in all experiments.

Core–shell Au@IONP synthesis procedure

Core–shell Au@IONPs were synthesized based on the method that has recently been published by Montazerabadi et al. [12]. Briefly, IONPs were synthesized using a modification of the co-precipitation method of Massart [23]. First, 12.5 mL of NH_3 (2 M) was added dropwise to a 2:1 solution of $FeCl_3.6H_2O$ and $FeCl_2.4H_2O$ under mechanical stirring. When the addition was completed, the sediment was separated by an external magnetic field, washed three times with methanol, dispersed in 50 mL of toluene, and stored as the source of the IONP colloidal solution. Then, (3-aminopropyl)trimethoxysilane (APTMS) (25 μL) was added to12.5 mL of the IONPs and sonicated for 30 min. The solution was heated for 4 h at 60 °C in an oven. The sediment was separated by a magnetic field, washed three times with methanol to remove the extra APTMS and toluene, and dispersed in methanol.

To form the gold shell on the surface of the IONPs, AuNPs with a diameter less than 3 nm were prepared as detailed in the literature [24] and immobilized onto the surface of the APTMS-functionalized IONPs. For this purpose, 4 mL of APTMS-functionalized IONPs (51.5 mM Fe) in methanol was added dropwise to a 25 mL solution of undiluted AuNPs (0.198 mM Au). Next, 4 mL of methanol and 10 mL of water were added to maximize the coverage of AuNPs on

the IONP surface. After 2 h of stirring at room temperature, the AuNPs were immobilized onto the surface of the IONPs. The resulting nanoparticles were separated magnetically, washed three times with DI water, and dispersed in 15 mL of DI water. Finally, 0.011 g of chloroauric acid was added to the 15 mL solution of prepared Au immobilized on the IONP surface under sonication. To complete the shell formation, 0.4 mL (78.9 mM) of ascorbic acid was added. After 2 h of incubation, a continuous and complete Au shell layer was formed on the IONP surface.

Au@IONP characterization

To determine the shell thickness and size distribution of the core–shell nanocomplex, high-resolution transmission electron microscopy (HR-TEM) was performed on at least 50 individual Au@IONPs and the size of each particle was measured using ImageJ software (1.44 P, NIH, USA). The UV–visible (UV–Vis) absorption spectra of the Au@IONP dispersed in water were recorded using a Rayleigh UV-1601 instrument. The hydrodynamic size and zeta potential of Au@IONPs were measured using a Malvern instrument.

In vitro experiments

MRI relaxometry

Relaxometry refers to the measurement of the relaxation variables in MRI to determine the specific physical and chemical properties of materials. Solutions of Au@IONP were prepared in water at equivalent concentrations of 0.03, 0.06, 0.12, 0.25, 0.5, and 1 mM Fe for the relaxivity measurements. All measurements were conducted at room temperature using a 3-T MRI clinical scanner (Magnetotrio, Siemens). T_2 relaxivity was determined using spin-echo acquisition utilizing 32 echo-times (TE) ranging from 12 to 384 ms and a repetition time (TR) of 3000 ms. The other scan parameters were as follows:

Field of view 7 cm; slice thickness 3 mm; and acquisition matrix 256 × 128.

The ability of a contrast agent to enhance the proton relaxation rate is determined by the relaxivity (ri) which decreases the longitudinal and transverse relaxation times. The equations for the relaxivity of each contrast agent are as follows:

$$\left(\frac{1}{T_1}\right)_{Observed} = \left(\frac{1}{T_1}\right)_{intrinsic} + r_1 C \quad (1)$$

$$\left(\frac{1}{T_2}\right)_{Observed} = \left(\frac{1}{T_2}\right)_{intrinsic} + r_2 C \quad (2)$$

where T_1 and T_2 are the longitudinal and transversal relaxations, C is the concentration (molar) of the contrast agent, and r_1 and r_2 are the relaxivity constants of the agent. The relaxivity of the synthesized Au@IONPs was calculated by linear curve fitting of the relaxation rates of different concentrations versus concentration. Calculations were performed using Microsoft Excel software.

Cell culture

Human nasopharyngeal carcinoma cell line KB was purchased from the Pasteur Institute of Iran (Tehran, Iran). This cell line was maintained in Roswell Park Memorial Institute medium (RPMI-1640) (Gibco, NY, USA) supplemented with 10% fetal bovine serum (FBS) (Gibco, NY, USA), 300 U/mL of penicillin (Sigma-Aldrich, MO, USA), and 200 mg/L of streptomycin (Sigma-Aldrich, MO, USA). KB cells were cultured as a monolayer at a density of 10^4 cells/cm^2 in T-25 tissue culture flasks. The cultures were maintained at 37 °C in a humidified atmosphere of 5% CO_2.

Cytotoxicity assay

When the cells were 80% confluent, they were detached with trypsin-EDTA. The cells were then centrifuged at 200 *g* for 7 min and counted using trypan blue to determine viability. Cells were seeded at a density of 5000 cells/well and incubated with Au@IONPs at different concentrations (0 (control), 10, 25, and 50 μg/mL) in flat-bottom 96-well plates for 6 and 12 h. Then, the nanoparticles were removed and replaced with fresh culture medium supplemented with 10% FBS, and the plate was kept in CO_2 incubator overnight (24 h is often used as an incubation period in the evaluation of cytotoxicity effects of chemical agents because of the direct effects of these agents on cells [25]). The retention of regenerative potential was estimated using the MTT-tetrazolium assay, which measures the ability of metabolically active mitochondria in live cells to reduce a colorless tetrazolium compound to a blue formazan product. To perform this assay, the culture medium was removed, 100 mL of culture medium without FBS and 10 mL of MTT (5 mg/mL in PBS) were added to each well, and the plate was returned to the incubator. After 4 h, the medium was removed from the wells, and the cells were lysed with 200 mL of DMSO. After the formazan product was dissolved, the absorbance at 570 nm was measured using an ELISA reader (Stat Fax-2100 Awareness, Mountain View, CA, USA). The relative survival was represented as the absorbance of the treated sample divided by absorbance of the control group. Eight replicates were used for each condition, and the experiments were repeated at least three times.

Photothermal treatment

In addition to the previous step, KB cells were seeded at a density of 10^4 cells/well and incubated with Au@IONP at

different concentrations (0 (control), 10, 25, and 50 μg/mL) in flat-bottom 96-well plates for 6 and 12 h. Then, the nanoparticles were removed and replaced with fresh culture medium. Each well was separately irradiated by an 808-nm laser (Nanobon Company, Tehran, Iran) with a power density of 6.3 W/cm^2 for 5 min. The light spot covered 1 well, which was considered as one experimental group. Following the photothermal treatment, the cells were relocated to the incubator for overnight. It should be noted that sufficient control groups were considered for the Au@IONP complex and light exposure, separately.

Thermometry

In this section of study, temperature distributed in each well of a microplate during photothermal therapy process was measured. KB cells were seeded in 96-well cell culture microplate at a density of 10^4 cells/well and incubated for 24 h at 37 °C in a humidified 5% CO_2 atmosphere. The medium solution containing Au@IONP nanocomplex (at concentration of 50 μg/mL) was prepared and added to the cells. After 6 h incubation, the culture medium was removed. The cells were washed twice with PBS to remove unloaded nanoparticles, and then fresh medium was added. The 96-well microplate was placed on a warm surface at constant temperature of 37 °C. After reaching thermal equilibrium between the warm surface and 96-well microplate, the cells were irradiated by laser. Laser exposure conditions were selected similar to what reported for in the previous section. The distance between the plate and laser source was set to cover the entire surface of a well. Temperature variations of the cells were monitored with a digital infrared thermal camera (Testo 875-1i, Germany) during laser irradiation.

Statistical analysis

The results are expressed as the mean values ± SEM (standard error of mean). Statistical analysis was performed using a one-way analysis of variance (ANOVA) followed by Tukey's test as the post-hoc analysis using SPSS version 12. A value of $P < 0.05$ was considered to be significant.

Results

According to Fig. 1a, the size distribution of the synthesized core–shell Au@IONP nanocomplex ranges from 20 to 50 nm and the highest frequency is located at 33 nm. The zeta

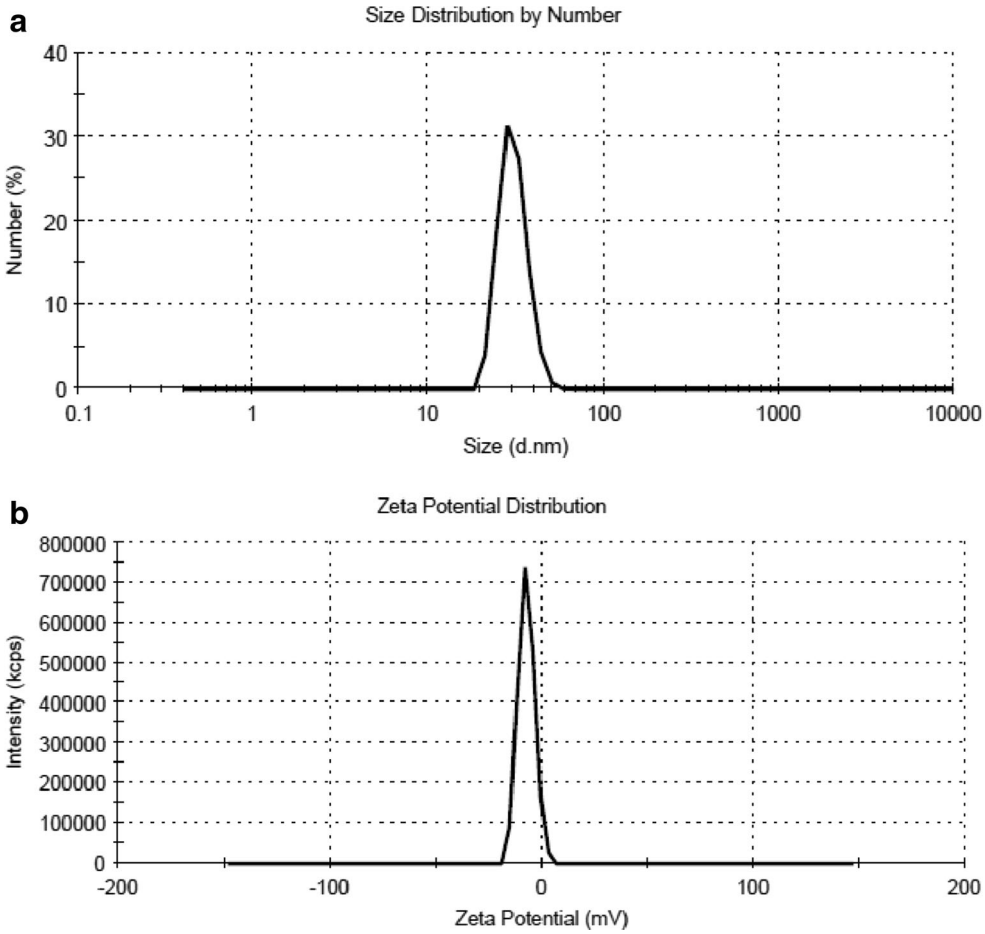

Fig. 1 (**a**) Size distribution of the synthesized Au@IONPs. (**b**) Zeta potential distribution of the synthesized Au@IONPs

potential of nanocomplex is shown in Fig. 1b in which one may find the surface potential of nanoparticles is −7.73 mV.

Figure 2 shows the UV–Vis spectra obtained at different steps of the nanoparticle synthesis procedure to confirm the formation of a complete core–shell. Figure 2a and b shows the UV–Vis spectra of the IONPs and the AuNPs, respectively. The UV–Vis spectral curve of the core–shell nanoparticles is presented in Fig. 2c. According to Fig. 2c, the surface plasmon resonance band for the Au@IONPs shows a red-shift and broadening of the peak in comparison with the AuNPs, which is commonly observed in other Au bimetallic systems [26].

Figure 3 shows TEM images of core–shell Au@IONPs in which a dense uniform coating of Au on the IONP surface is visible. Additionally, it is observable from Fig. 3 that the core size of the Au@IONP and the gold shell thickness are less than 30 and 5 nm, respectively.

Based on our MR relaxometry experiments and Eqs. (1) and (2), it was revealed that the longitudinal and transverse relaxivities of the synthesized core–shell Au@IONP are 0.87 mM^{-1} S^{-1} and 95.03 mM^{-1} S^{-1}, respectively (Fig. 4a and b).

We investigated the cytotoxicity effects of the core–shell Au@IONP on KB cells in various concentrations ranging from 0 to 50 μg/mL. Furthermore, cytotoxicity was investigated for different incubation periods of 6 and 12 h. The results achieved by performing cytotoxicity tests on KB cells are demonstrated in Figs. 5 and 6. According to these figures, no significant cytotoxicity is observed at concentration of 10 μg/mL and a moderate cytotoxicity was seen at the higher nanoparticle concentrations. To study the effect of the laser on KB cells, different exposure times (from 2 to 20 min) were examined and the laser was used to irradiate the cells in the absence of nanoparticles. These examinations were conducted to observe how the exposure time changes the percentage of KB cell survival. We observed that a 20-min laser exposure induces significant cell death while no significant cell lethality took place when an exposure time of 5 min was applied.

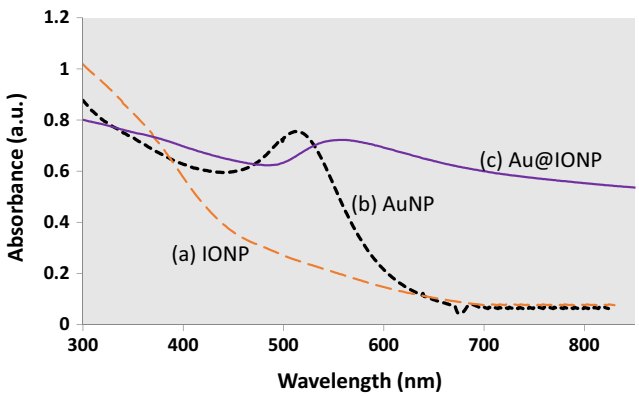

Fig. 2 UV–visible spectra of different nanoparticles: (**a**) IONPs, (**b**) AuNPs, and (**c**) the synthesized Au@IONP core–shell

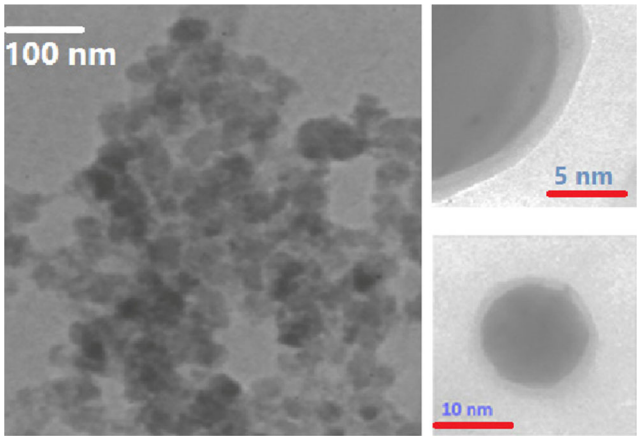

Fig. 3 High-resolution transmission electron microscope images of the synthesized Au@IONP nanocomplex

Accordingly, we selected 5 min as the exposure time for all nanophoto-thermal treatment procedures.

A significant difference is found between non-irradiated samples and irradiated samples in terms of cell viability ($P < 0.05$ for each Au@IONP concentration). Figure 5 shows that the viability of KB cells exposed to Au@IONP at concentrations of 0, 10, 25, and 50 μg/mL without laser

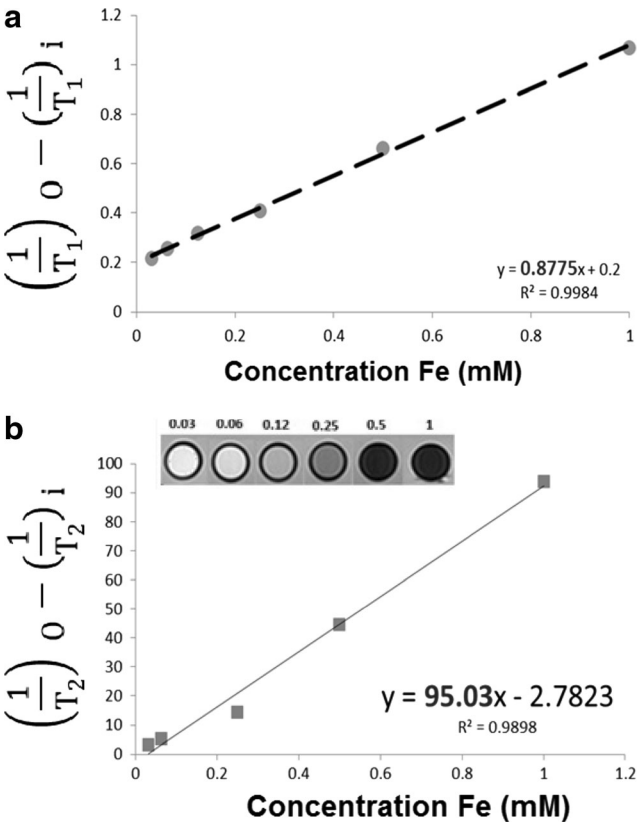

Fig. 4 (**a**) Longitudinal relaxation rates versus concentration of Fe (mM) for the synthesized Au@IONP nanocomplex ("o" stands for "observed" and "i" stands for "intrinsic"). (**b**) Transverse relaxation rates versus concentration of Fe (mM) for the synthesized Au@IONP nanocomplex ("o" stands for "observed" and "i" stands for "intrinsic")

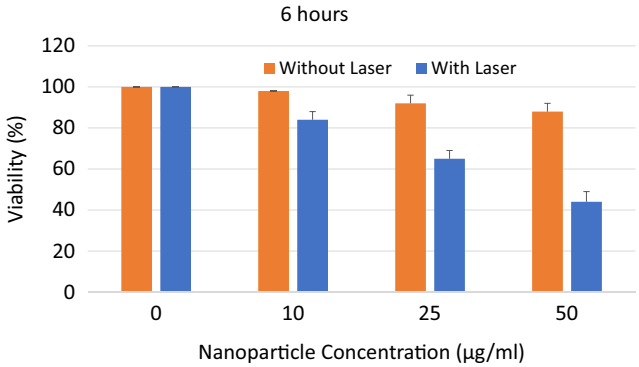

Fig. 5 Viability of KB cells incubated with different concentrations of Au@IONPs for 6 h with and without receiving a laser exposure

irradiation changes from 100 to 98, 92, and 88%, respectively. These percentages are reduced to 84, 65, and 44% when the laser was used to irradiate the KB cells. The effects of incubation time on the photothermal treatment are observable in Fig. 6. According to Fig. 6, it is found that the viability of KB cells exposed to Au@IONPs at concentrations of 0, 10, 25, and 50 μg/mL for 12 h without laser irradiation changes from 100 to 93, 86, and 80%, respectively. These percentages are respectively reduced to 76, 53, and 31% when the laser was used to irradiate the KB cells.

In the next section of this study, we studied the thermal distribution profile of KB cells treated with nanophotothermal method. The background temperature was approximately 37 °C. As seen in Fig. 7a, temperature of each well containing nanocomplex is lower than background. The reason seems to be relevant to the presence of water in these wells. When the laser is used to irradiate the well containing KB cells in the absence of nanocomplex, it was observed that temperature increased to 39.7 °C (Fig. 7b). Laser irradiation to the KB cells incubated with nanocomplex caused ~10 °C increase in temperature (Fig. 7c). This experiment shows that temperature is distributed homogeneously in each well receiving nanophoto-thermal therapy.

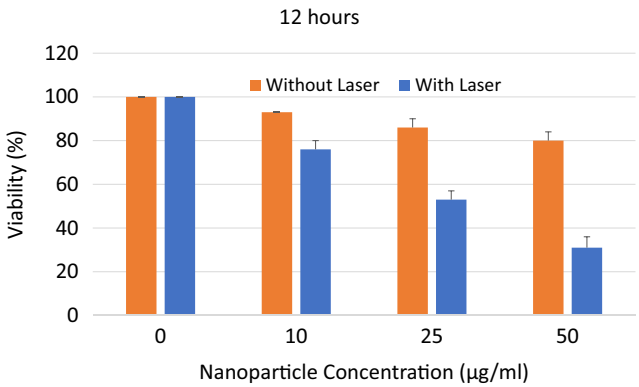

Fig. 6 Viability of KB cells incubated with different concentrations of Au@IONPs for 12 h with and without receiving a laser exposure

Discussion

As shown in Figs. 1 and 3, the synthesized nanocomplex is spherical in shape and the size of nanoparticles is smaller than 40 nm. TEM and UV–visible spectrum of nanocomplex confirmed the formation of gold shell. To form an appropriate Au shell, two steps were considered. In the first step of the synthesis, the fine AuNPs (<3 nm) were conjugated to amine groups presented on the surface of IONPs. In the second step, we used Au^{3+} ions and ascorbic acid as a well-known mild reducing agent [22]. In this step, ascorbic acid reduces Au^{3+} to Au^{1+} ions and finally Au^{1+} ions are reduced to Au atoms by those fine AuNPs presented on the surface of IONPs. The process of reduction of Au ions is very slow and controllable. As a result, a uniform Au shell was formed (Fig. 3). Thickness of Au shell may be directly adjusted by the amount of Au ions used in the reaction.

It was also found that zeta potential of nanocomplex is of −7.73 mV, and such a potential is not good enough to keep the particles from clustering together. As a result, incipient instability of the nanocomplex must be modified. Surface coating of the nanocomplex with poly-ethylene-glycol (PEG) is one of the best solutions to increase the stability and solubility of the nanocomplex [12].

As shown in Fig. 2, a characteristic surface plasmon resonance peak clearly occurs near 600 nm for Au@IONPs. This is the characteristic absorption property of gold nanoshells, ensuring that the gold nanoshell structure was successfully formed. The biocompatibility assessment of Au@IONPs even at highest used concentration (50 μg/mL) and longest incubation period (12 h) shows a cell viability of 80%, demonstrating that Au@IONPs induce low cytotoxicity in KB cells. Moreover, the evident darkening of MR images is observed with increases in iron concentration. The finding of the MRI relaxometry experiments confirms the T_2-enhancing capability of Au@IONPs, making them useful contrast agents for MRI.

Current clinically used thermal ablation methods utilize various sources of energy such as radiofrequency waves, microwaves, ultrasound, and alternative magnetic fields [27]. These thermal therapy approaches have two major common limitations including nonspecific heating of targeted tissues and potential injury to surrounding healthy tissues. Photothermal ablation approaches may provide improved tumor-specific heating with new and emerging nanomaterials aiding to photosensitize the targeted tissues. Here, we prepared iron oxide-core gold shell nanoparticles and applied such nanoparticles in photothermal therapy of KB cells. Au@IONPs were internalized in KB cells and permitted photothermal ablation in a controllable manner with decreasing cell viability dependent upon some variables.

In practice, we investigated the role of two factors on the efficacy of the photothermal ablation of KB cells: (1) the

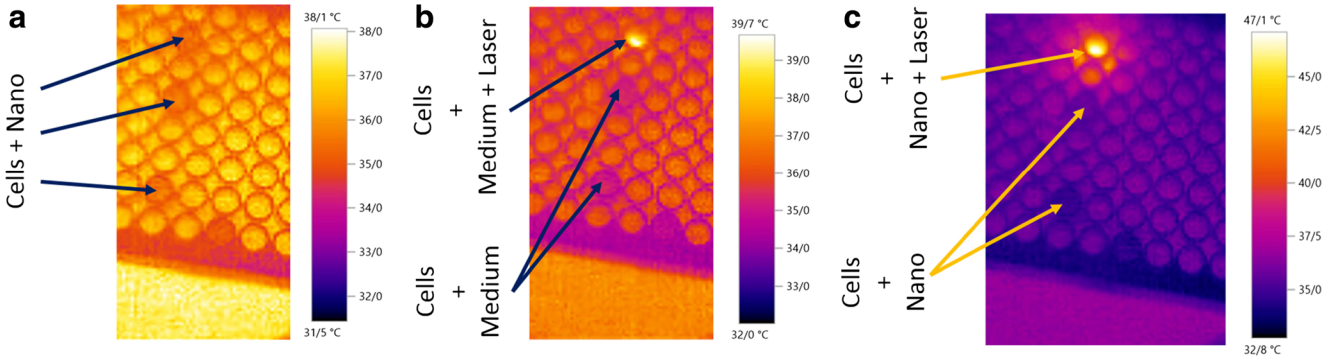

Fig. 7 Thermal distribution profile of a 96-well microplate containing KB cells treated by (**a**) the nanocomplex, (**b**) laser, and (**c**) a combination of the nanocomplex and laser

effect of nanoparticle concentration and (2) the effect of the incubation time of nanoparticles with KB cells. The highest level of cell death following 5 min laser irradiation is observed at a nanoparticle concentration of 50 μg/mL and an incubation time of 12 h. According to our in vitro experiments, we conclude that longer incubation time may be preferred over using higher concentrations of nanoparticles to reach a higher level of cell death. Similar observations have been reported in several prior studies using various gold nanomaterials as photothermal agents for the ablation of human prostate cancer cells, murine renal carcinoma cells, mouse fibroblast cells, and human breast cancer cells [28, 29].

It has been recently confirmed that when NIR laser is utilized, the corresponding energy absorption values in this wavelength range for Au@IONP are directly converted to heat that may result in a good heating profile. The Au shell is the component responsible for the NIR absorption and resulted in the cell damage by this nanocomplex. However, bare Fe_3O_4 nanoparticles did not show absorption peaks in the area of NIR, and no heating may be achieved following NIR laser irradiation [28]. Gue et al. have demonstrated that the temperature increases relatively slowly from 8 to 13 °C for PANC-1 cells receiving NIR irradiation alone. They also have demonstrated that temperature changes during NIR irradiation (power density 3.2 W/cm^2) are increased dramatically from 7 to 60 °C when the PANC-1 cells are incubated with 25 μg/mL of Au@IONP for 24 h [28].

On the other hand, various image-guided thermal therapy methods have been widely promoted with current imaging modalities such as X-ray computed tomography, optical imaging, and MRI [30–32]. However, X-ray computed tomography uses ionizing radiation to form an image and safety considerations would limit the human studies. Depth penetration issues in optical imaging limit the applications of this modality to only superficial tissue examinations. As a result, MRI may offer the greatest potential for clinical translation. The integration of MRI and photothermal therapy for cancer allows the physicians to potentially adjust laser irradiation parameters (power density and duration) based upon MRI assessments of nanoparticle deposition within the targeted tumor tissues.

The current study reveals the effectiveness of using core–shell Au@IONPs as a potent MRI-visible photosensitizer during the laser irradiation of cancer cells. There have also been some other studies showing that other types of nanoparticles can perform similarly well for these types of applications [28, 33]. The noticeable combination of properties of IONPs and AuNPs with the local application of NIR laser irradiation offers a promising approach for the photothermal ablation therapy of nasopharyngeal carcinoma [16, 34]. MRI studies demonstrated that Au@IONPs may be utilized as a good T_2 contrast agent, and it is expected that nasopharyngeal carcinoma may be better observed if Au@IONPs are internalized into cancer cells.

Considering the promising initial results obtained for the synthesized Au@IONPs in the current in vitro study and some other relevant reports published by other people [35], a reasonable scenario may be proposed for efficient diagnosis and therapy of cancers, particularly head and neck carcinomas. Vogl et al. reported their clinical data on six patients with nasopharyngeal tumors receiving laser-induced thermotherapy (LITT). They detected the margins of the tumors using MRI and then utilized laser irradiation to treat the patients. Laser light was transmitted to cancer tissues using an optical fiber. Also, Vogl et al. used MRI to obtain information about thermal dose distribution when the LITT process was performed [35]. Combination of Au@IONPs with the work done by Vogl et al. may be led to (a) more sensitive detection of cancer lesions using MRI (because of the presence of magnetic nanoparticles in the Au@IONP nanocomplex) and (b) enhancement of laser therapy efficacy (because of the presence of AuNPs in the Au@IONP nanocomplex). This scenario may led to better output if early detected nasopharyngeal tumors are considered as the targets, because such tumors have high chances for laser therapies [36, 37]. To achieve a rapid test for early detection of nasopharyngeal tumors, we have recently produced a nanotechnology-based immuno-chromatographic assay kit with good sensitivity and specificity for screening this type of carcinomas [38].

Considering all potentials stated above, we may be able to detect nasopharyngeal carcinomas at early stages, identify the cancer lesions using MRI and Au@IONP (as a contrast agent), and try to treat the early detected nasopharyngeal tumors with a higher chance. This way, we believe nanomedicine may hold great promises to increase the efficiency of cancer diagnosis and therapy. Certainly, additional investigations are needed to rigorously examine the potential therapeutic efficacy of the presented approach with in vivo preclinical animal model studies. It is also expected the suggested approach may overcome the limitations of current thermal ablation methods by limiting unwanted damage to adjacent normal tissues.

Conclusions

We report the synthesis and characteristics of core–shell Au@IONPs using APTMS as a linker between Au and the IONP. UV–visible spectroscopy and TEM confirm the formation of layered core–shell Au@IONPs. Because this synthesized nanocomplex contains IONPs, it can be applied to MR imaging as a new contrast agent. The significant light absorption of this new synthesized nanocomplex makes it a promising material for use in cancer photothermal therapy or the thermal ablation of tumors.

The conclusion of our experiments may be summarized as follows:

- The synthesized core–shell Au@IONPs are an appropriate MRI contrast agent.
- This nanocomplex may be considered relatively safe to cells even for a long period of incubation time.
- This nanocomplex can be heated to the desired temperature level through exposure to an 808 nm laser according to the procedure introduced in this report.
- The results of our studies show that the nanocomplex concentration plays an important role in the photothermal cell destruction.
- Our findings show the process of the nanocomplex entering the cells is strongly time-dependent.

Compliance with ethical standards This research did not involve human participants and/or animals.

Conflict of interest statement The authors declare that they have no conflicts of interest.

References

1. Shakeri-Zadeh A, Mansoori GA, Hashemian AR, Eshghi H, Sazgarnia A, Montazerabadi AR (2010) Cancerous cells targeting and destruction using folate conjugated gold nanoparticles. Dyn Biochem Process Biotechnol Mol Biol 4(1):06–12
2. Sazgarnia A, Montazerabadi AR, Bahreyni-Toosi MH, Ahmadi A (2013) Photosensitizing and radiosensitizing effects of mitoxantrone: combined chemo-, photo-, and radiotherapy of DFW human melanoma cells. Lasers Med Sci 28(6):1533–1539
3. Peer D, Karp JM, Hong S, Farokhzad OC, Margalit R, Langer R (2007) Nanocarriers as an emerging platform for cancer therapy. Nat Nanotechnol 2(12):751–760
4. Ferrari M (2005) Cancer nanotechnology: opportunities and challenges. Nat Rev Cancer 5(3):161–171
5. Beik J, Abed Z, Shakeri-Zadeh A, Nourbakhsh M, Shiran MB (2016) Evaluation of the sonosensitizing properties of nanographene oxide in comparison with iron oxide and gold nanoparticles. Physica E: Low-dimensional Systems and Nanostructures 81: 308–314
6. Khoei S, Mahdavi SR, Fakhimikabir H, Shakeri-Zadeh A, Hashemian A (2014) The role of iron oxide nanoparticles in the radiosensitization of human prostate carcinoma cell line DU145 at megavoltage radiation energies. Int J Radiat Biol 90(5):351–356
7. Mansoori GA, Brandenburg KS, Shakeri-Zadeh A (2010) A comparative study of two folate-conjugated gold nanoparticles for cancer nanotechnology applications. Cancers 2(4):1911–1928
8. Beik J, Abed Z, Ghadimi-Daresajini A, Nourbakhsh M, Shakeri-Zadeh A, Ghasemi MS et al (2016) Measurements of nanoparticle-enhanced heating from 1MHz ultrasound in solution and in mice bearing CT26 colon tumors. J Therm Biol 62:84–89
9. Shakeri-Zadeh A, Khoee S, Shiran M-B, Sharifi AM, Khoei S (2015) Synergistic effects of magnetic drug targeting using a newly developed nanocapsule and tumor irradiation by ultrasound on CT26 tumors in BALB/c mice. J Mater Chem B 3(9):1879–1887
10. Shakeri-Zadeh A, Khoei S, Khoee S, Sharifi AM, Shiran M-B (2015) Combination of ultrasound and newly synthesized magnetic nanocapsules affects the temperature profile of CT26 tumors in BALB/c mice. Journal of Medical Ultrasonics 42(1):9–16
11. Shakeri-Zadeh A, Shiran M-B, Khoee S, Sharifi AM, Ghaznavi H, Khoei S (2014) A new magnetic nanocapsule containing 5-fluorouracil: in vivo drug release, anti-tumor, and pro-apoptotic effects on CT26 cells allograft model. J Biomater Appl 29(4):548–556
12. Montazerabadi AR, Oghabian MA, Irajirad R, Muhammadnejad S, Ahmadvand D, Delavari HH et al (2015) Development of gold-coated magnetic nanoparticles as a potential MRI contrast agent. Nano 10(04):1550048
13. Chouly C, Pouliquen D, Lucet I, Jeune J, Jallet P (1996) Development of superparamagnetic nanoparticles for MRI: effect of particle size, charge and surface nature on biodistribution. J Microencapsul 13(3):245–255
14. Gupta AK, Gupta M (2005) Synthesis and surface engineering of iron oxide nanoparticles for biomedical applications. Biomaterials 26(18):3995–4021
15. Mehdizadeh A, Pandesh S, Shakeri-Zadeh A, Kamrava SK, Habib-Agahi M, Farhadi M et al (2014) The effects of folate-conjugated gold nanorods in combination with plasmonic photothermal therapy on mouth epidermal carcinoma cells. Lasers Med Sci 29(3):939–948
16. Shakeri-Zadeh A, Kamrava SK, Farhadi M, Hajikarimi Z, Maleki S, Ahmadi A (2014) A scientific paradigm for targeted nanophotothermolysis; the potential for nanosurgery of cancer. Lasers Med Sci 29(2):847–853
17. Aioub M, El-Sayed MA (2016) A real-time surface enhanced Raman spectroscopy study of plasmonic photothermal cell death using targeted gold nanoparticles. J Am Chem Soc 138(4):1258–1264
18. Huang X, El-Sayed MA (2011) Plasmonic photo-thermal therapy (PPTT). Alexandria Journal of Medicine 47(1):1–9
19. Huang X, Jain PK, El-Sayed IH, El-Sayed MA (2008) Plasmonic photothermal therapy (PPTT) using gold nanoparticles. Lasers Med Sci 23(3):217

20. Hoshyar N, Gray S, Han H, Bao G (2016) The effect of nanoparticle size on in vivo pharmacokinetics and cellular interaction. Nanomedicine 11(6):673–692
21. Liu Y, Yang M, Zhang J, Zhi X, Li C, Zhang C et al (2016) Human induced pluripotent stem cells for tumor targeted delivery of gold nanorods and enhanced photothermal therapy. ACS Nano 10(2): 2375–2385
22. Sood A, Arora V, Shah J, Kotnala R, Jain TK (2016) Ascorbic acid-mediated synthesis and characterisation of iron oxide/gold core–shell nanoparticles. J Exp Nanosci 11(5):370–382
23. Massart R (1981) Preparation of aqueous magnetic liquids in alkaline and acidic media. Magnetics, IEEE Transactions on 17(2): 1247–1248
24. Jana NR, Gearheart L, Murphy CJ (2001) Seeding growth for size control of 5–40 nm diameter gold nanoparticles. Langmuir 17(22): 6782–6786
25. Bagalkot V, Farokhzad OC, Langer R, Jon S (2006) An aptamer–doxorubicin physical conjugate as a novel targeted drug-delivery platform. Angew Chem Int Ed 45(48):8149–8152
26. Cheng G, Walker ARH (2007) Synthesis and characterization of cobalt/gold bimetallic nanoparticles. J Magn Magn Mater 311(1): 31–35
27. Beik J, Abed Z, Ghoreishi FS, Hosseini-Nami S, Mehrzadi S, Shakeri-Zadeh A et al (2016) Nanotechnology in hyperthermia cancer therapy: from fundamental principles to advanced applications. J Control Release 235:205–221
28. Guo Y, Zhang Z, Kim D-H, Li W, Nicolai J, Procissi D et al (2013) Photothermal ablation of pancreatic cancer cells with hybrid iron-oxide core gold-shell nanoparticles. Int J Nanomedicine 8:3437
29. Khafaji M, Vossoughi M, Hormozi-Nezhad MR, Dinarvand R, Börrnert F, Irajizad A (2016) A new bifunctional hybrid nanostructure as an active platform for photothermal therapy and MR imaging. Sci Rep 6
30. von Maltzahn G, Park J-H, Agrawal A, Bandaru NK, Das SK, Sailor MJ et al (2009) Computationally guided photothermal tumor therapy using long-circulating gold nanorod antennas. Cancer Res 69(9):3892–900
31. Melancon MP, Elliott A, Ji X, Shetty A, Yang Z, Tian M et al (2011) Theranostics with multifunctional magnetic gold nanoshells: photothermal therapy and T2* magnetic resonance imaging. Investig Radiol 46(2):132
32. de Senneville BD, Roujol S, Jaïs P, Moonen CT, Herigault G, Quesson B (2012) Feasibility of fast MR-thermometry during cardiac radiofrequency ablation. NMR Biomed 25(4):556–562
33. Ma LL, Feldman MD, Tam JM, Paranjape AS, Cheruku KK, Larson TA et al (2009) Small multifunctional nanoclusters (nanoroses) for targeted cellular imaging and therapy. ACS Nano 3(9):2686–2696
34. Samadian H, Hosseini-Nami S, Kamrava SK, Ghaznavi H, Shakeri-Zadeh A (2016) Folate-conjugated gold nanoparticle as a new nanoplatform for targeted cancer therapy. J Cancer Res Clin Oncol 142(11):2217–2229
35. Vogl TJ, Mack MG, Müller P, Phillip C, Böttcher H, Roggan A et al (1995) Recurrent nasopharyngeal tumors: preliminary clinical results with interventional MR imaging-controlled laser-induced thermotherapy. Radiology 196(3):725–733
36. Agostinis P, Berg K, Cengel KA, Foster TH, Girotti AW, Gollnick SO et al (2011) Photodynamic therapy of cancer: an update. CA Cancer J Clin 61(4):250–281
37. Wildeman MA, Nyst HJ, Karakullukcu B, Tan BI (2009) Photodynamic therapy in the therapy for recurrent/persistent nasopharyngeal cancer. Head & neck oncology 1(1):40
38. Goudarzi S, Ahmadi A, Farhadi M, Kamrava SK, Mobarrez F, Omidfar K (2015) A new gold nanoparticle based rapid immunochromatographic assay for screening EBV-VCA specific IgA in nasopharyngeal carcinomas. J Appl Biomed 13(2):123–129